

Solution Structure of an Intramembrane Aspartyl Protease via Small Angle Neutron Scattering

Swe-Htet Naing,¹ Ryan C. Oliver,² Kevin L. Weiss,² Volker S. Urban,^{2,*} and Raquel L. Lieberman^{1,*}

¹School of Chemistry and Biochemistry, Georgia Institute of Technology, Atlanta, Georgia and ²Neutron Scattering Division, Oak Ridge National Laboratory, Oak Ridge, Tennessee

ABSTRACT Intramembrane aspartyl proteases (IAPs) comprise one of four families of integral membrane proteases that hydrolyze substrates within the hydrophobic lipid bilayer. IAPs include signal peptide peptidase, which processes remnant signal peptides from nascent polypeptides in the endoplasmic reticulum, and presenilin, the catalytic component of the γ -secretase complex that processes Notch and amyloid precursor protein. Despite their broad biomedical reach, basic structure-function relationships of IAPs remain active areas of research. Characterization of membrane-bound proteins is notoriously challenging due to their inherently hydrophobic character. For IAPs, oligomerization state in solution is one outstanding question, with previous proposals for monomer, dimer, tetramer, and octamer. Here we used small angle neutron scattering (SANS) to characterize *n*-dodecyl- β -D-maltopyranoside (DDM) detergent solutions containing and absent a microbial IAP ortholog. A unique feature of SANS is the ability to modulate the solvent composition to mask all but the enzyme of interest. The signal from the IAP was enhanced by deuteration and, uniquely, scattering from DDM and buffers were matched by the use of both tail-deuterated DDM and D₂O. The radius of gyration calculated for IAP and the corresponding *ab initio* consensus model are consistent with a monomer. The model is slightly smaller than the crystallographic IAP monomer, suggesting a more compact protein in solution compared with the crystal lattice. Our study provides direct insight into the oligomeric state of purified IAP in surfactant solution, and demonstrates the utility of fully contrast-matching the detergent in SANS to characterize other intramembrane proteases and their membrane-bound substrates.

INTRODUCTION

Intramembrane proteases (IPs) cleave membrane-embedded substrates within the confines of the lipid bilayer. Products of IPs are peptides and proteins involved in various biochemical processes such as cell metabolism, differentiation, development, immune response, and surveillance (1), and IPs are drug targets for a number of diseases (2). IPs are categorized by their nucleophile: serine, cysteine, aspartate, or their metal ion requirement (2–5). Intramembrane aspartyl proteases include presenilin and signal peptide peptidase (SPP). Presenilin is the catalytic component of γ -secretase responsible for generating amyloid- β (A β) peptides implicated in Alzheimer's disease from amyloid precursor protein (3,5), and SPP cleaves remnant leader peptides in the endoplasmic reticulum membrane after cleavage by the soluble signal peptidase (6). In humans, SPP substrates include

leader peptides from proteins involved in immune system, inflammatory response, and hepatitis C viral maturation (7–9). SPP and presenilin share key sequence and catalytic similarity, including signature catalytic motifs (YD and GxGD where x is any amino acid) and inhibition (10–13); similarities extend to microbial orthologs (12–14).

Despite their broad biomedical reach, the structure of active intramembrane aspartyl proteases (IAPs) including the number of subunits in the functional enzyme, has remained ambiguous. Membrane proteins require the presence of a mild detergent or other amphiphilic system to solubilize and stabilize a given membrane protein in an active conformation, which hinders structural characterization using standard analytical techniques used for soluble proteins such as size exclusion chromatography or small angle x-ray scattering (SAXS). In the case of size exclusion chromatography, even coupled with multiangle light scattering, molecular mass determination is only possible when the protein-detergent complex is well separated from empty micelles (15), and in SAXS, the signal from the membrane protein cannot be isolated from that of the solubilizing agent (16). For IAPs, stoichiometries of one

Submitted October 26, 2017, and accepted for publication December 18, 2017.

*Correspondence: urbanvs@ornl.gov or raquel.lieberman@chemistry.gatech.edu

Swe-Htet Naing and Ryan C. Oliver contributed equally to this work.

Editor: James Cole.

<https://doi.org/10.1016/j.bpj.2017.12.017>

© 2017 Biophysical Society.

(17) through eight (18) subunits have been proposed. Before recent cryo-electron microscopy studies of γ -secretase that indicate a monomer (17), homodimer (19–23) was the predominant proposal. Fluorescence lifetime imaging microscopy was used to demonstrate that both SPP (21,22) and presenilins (19,20) are dimers. The lattice arrangement of the 3.8 Å resolution crystal structure of the microbial *Methanococcus marisnigri* IAP (WP_011844759.1, MmIAP) ortholog suggests either a dimer or tetramer (24).

To date, no IP has been structurally characterized using small angle neutron scattering (SANS), a method well suited to study the solution properties of macromolecules and complex multicomponent assemblies like membrane proteins (25). For membrane protein-detergent complexes, the different scattering length densities of each component can be exploited so that only the membrane protein is visualized during the scattering experiment. Typically, the scattering length densities of the detergent and buffer/solvent are matched by judiciously adjusting the ratio of H₂O and D₂O in the solvent (26), and the signal from the membrane protein can be further enhanced by deuteration during cell growth (25).

Here we report the solution structure of deuterated MmIAP in *n*-dodecyl- β -D-maltopyranoside (DDM) determined by SANS. After deuteration of MmIAP, the detergent was fully contrast-matched using a specific ratio of hydrogenated and tail-deuterated detergent, and the scattering profile for MmIAP was recorded. The radius of gyration (R_g) calculated for MmIAP from SANS is smaller than the R_g calculated from the crystallographic MmIAP monomer, suggesting a more compact protein in DDM-containing solution. Our SANS study provides, to our knowledge, new insight into the solution oligomeric state of MmIAP in detergent solution, and bolsters the utility of SANS to characterize other IPs and their membrane-bound substrates.

MATERIALS AND METHODS

Expression and purification of protonated and deuterated MmIAP

The plasmid containing the MmIAP gene with a C-terminal hexahistidine tag was transformed into *Escherichia coli* Rosetta 2 cells (Novagen, Madison, WI). Cells were grown, membranes isolated, and protein purified as described previously for enzyme activity assays (14). Modest modifications were made to scale purification to the higher protein requirement for SANS experiments. Membrane (~2 g) was solubilized in 160 mL of 50 mM Hepes (pH 7.5), 500 mM NaCl, 20 mM imidazole, and 1% (w/v) DDM (Anatrace, Maumee, OH) by gentle rocking for 1 h at 4°C. Unsolubilized material was removed via ultracentrifugation at 162,000 \times g for 45 min. The supernatant containing solubilized membranes was loaded onto a 1 mL HisTrap FF Crude nickel affinity chromatography column (GE Healthcare, Chicago, IL) pre-equilibrated with Buffer A [50 mM Hepes (pH 7.5), 500 mM NaCl, 20 mM imidazole, 0.1% DDM]. Before elution of MmIAP, weakly bound impurities were removed with 5% Buffer B [50 mM Hepes (pH 7.5), 500 mM NaCl, 500 mM imidazole, 0.1% DDM]. Elution of purified MmIAP was accomplished using a linear gradient by mixing

Buffer A and 5–60% Buffer B. Elution fractions containing MmIAP were pooled and further purified on a HiPrep 16/60 Sephacryl-S300 (GE Healthcare) using gel filtration buffer [20 mM Hepes (pH 7.5), 250 mM NaCl, 0.05% DDM]. Purity of protein was assessed by denaturing sodium dodecyl sulfate polyacrylamide gel electrophoresis analysis (12% polyacrylamide) stained with Coomassie and concentration was measured using a NanoDrop spectrophotometer (Thermo Scientific, Waltham, MA) ($\epsilon = 33,920 \text{ M}^{-1} \text{ cm}^{-1}$). Before SANS measurements, pure (protonated) MmIAP was buffer-exchanged using a 500 μ L Amicon Ultra MWCO 50K concentrator (Millipore, Burlington, MA) into gel filtration buffer containing 22% D₂O (Acros Organic, Geel, Belgium).

Fed-batch cultivation, expression of deuterated MmIAP (*d*-MmIAP), and cell lysis was carried out in the Bio-Deuteration Laboratory at Oak Ridge National Laboratory (ORNL, Oak Ridge, TN). Before *d*-MmIAP production, *E. coli* Rosetta 2 cells were first adapted to D₂O by transferring an individual colony of transformed cells from a Luria Broth agar plate to 0.5% (w/v) glycerol minimal medium in H₂O, and then subculturing into the same medium with an increasing D₂O content (25, 50, 75, and 90%), 100 μ g/mL carbenicillin, and 17 μ g/mL chloramphenicol. Once the cells were growing in 90% D₂O medium, a 400 mL preculture was used to inoculate 3.6 L of fresh 90% D₂O medium in a benchtop BioFlo 310 bioreactor system (Eppendorf, Hauppauge, NY) equipped with a 5.5 L working volume vessel. At the outset of the experiment, the temperature was maintained at 30°C, aeration was maintained throughout at 4 L/min, and agitation was varied from 200 to 800 Rpm to maintain dissolved oxygen above a set point of 30% saturation. A solution of 10% (w/v) NaOH in 90% D₂O was added on demand to maintain a pD >7.3. When the dissolved oxygen spike occurred upon depletion of the 0.5% (w/v) glycerol, a feeding of a solution consisting of 10% (w/v) glycerol and 0.2% MgSO₄ in 90% D₂O was initiated. After ~7 h of feeding, the temperature set point was reduced to 18°C and *d*-MmIAP expression was induced by adding 1 mM isopropyl- β -D-1-thiogalactopyranoside. Upon harvesting via centrifugation at 6000 \times g for 45 min, cell paste containing *d*-MmIAP (~145 g wet cell weight) was suspended (0.1 g/mL) in 50 mM Hepes (pH 7.5) and 200 mM NaCl containing EDTA-Free SIGMAFAST Protease Inhibitor Cocktail Tablets (Sigma Aldrich, St. Louis, MO), and lysed at 15,000 psi via three passages through an EmulsiFlex-C3 homogenizer that was fitted with a chilled heat exchanger (Avestin, Ottawa, ON) and stationed in a 6°C cold room. After lysis, cellular debris was removed by centrifugation at 5000 \times g for 15 min for four times. The supernatant (~1.8 L) was then subjected to ultracentrifugation at 162,000 \times g for 30 min. The pelleted membrane fraction was washed by resuspension in a Dounce homogenizer and the membrane fraction was again isolated by ultracentrifugation as above. *d*-MmIAP-containing membranes (~22 g) were solubilized by gentle rocking for 0.5 h at 4°C in 200 mL of a solution containing 50 mM Hepes (pH 7.5), 500 mM NaCl, 20 mM imidazole, and 4% (w/v) DDM. The membrane resuspension was subjected to ultracentrifugation as above to remove insoluble material.

The supernatant containing the solubilized membrane was purified using the protocol for MmIAP described above except for the following additional steps to maximize yield of purified enzyme. Namely, the flow through fractions from the first nickel affinity chromatography run were diluted in Buffer A lacking detergent, to a final concentration of 2% DDM, and purified on the column again. A third round of nickel affinity chromatography was then performed on the flow through from the second column, which was diluted with Buffer A lacking detergent to 1% DDM. Elution fractions from the three nickel affinity purification runs were pooled, concentrated to two ~900 μ L aliquots using a 15 mL Amicon Ultra MWCO 50K concentrator (Millipore), and each loaded onto a HiPrep 16/60 Sephacryl-S300 (GE Healthcare) pre-equilibrated as for MmIAP above. Fractions containing purified *d*-MmIAP as judged by sodium dodecyl sulfate polyacrylamide gel electrophoresis were pooled and a third Sephacryl-S300 column was used to further polish the sample. In a final step, purified *d*-MmIAP was loaded onto a Superose-12 10/300 GL (GE Healthcare) column equilibrated with 20 mM Hepes (pH 7.5), 250 mM NaCl, 48.5% D₂O, and 0.05% total DDM, of which 44% (w/v) is tail-deuterated d25-DDM (Anatrace)

(Fig. S1). The final yield was ~ 1 mg of *d*-MmIAP, all of which was used in the SANS experiment.

SANS data collection

SANS data were collected at the Bio-SANS beam line CG-3 of the High-Flux Isotope Reactor at ORNL using a single instrument configuration with 7-meter sample-to-detector distance. Data were collected at 12°C using 1 mm quartz cells and neutron wavelength of $6 \text{ \AA} \pm 14\%$. The range of momentum transfer Q used was $0.007 < Q < 0.7 \text{ \AA}^{-1}$ ($Q = 4\pi \times \sin(\theta)/\lambda$, where 2θ is the scattering angle and λ is the neutron wavelength). Additional descriptions of the instrument and setup have been previously published (27–29). The recorded scattering data were circularly averaged, and reduced to one-dimensional scattering profiles using MantidPlot software (30). Calibration of the SANS data to an absolute scale was performed by measuring a porous silica standard with known intensity at zero angle (extrapolated from a Debye-Bueche plot). Blank buffers containing the same percentage D₂O as the samples were similarly measured and subtracted from the sample scattering for background correction using a toolkit developed by Dr. Ken Littrell (ORNL) for IgorPro. Subsequent data analysis and modeling of scattering profiles were facilitated with the ATSAS 2.6.1 program suite (European Molecular Biology Laboratory, Hamburg) (31).

SANS data analysis and modeling

An initial estimation of the R_g and forward scattering intensity (I_0) was performed using PRIMUS (32). Core-shell ellipsoid shape models were fit to the scattering data using SasView v4.1 (33). Comparisons of SANS data for *d*-MmIAP to structures of MmIAP and presentin in the PDB were conducted with CRYSON (34). For the simulation conditions, a deuteration fraction of 0.75 was used for the protein chain with a D₂O fraction in the solvent of 0.49 to mimic the experimental contrast conditions.

ATSAS software tools were used for further modeling and interpretation of the structural SANS information for *d*-MmIAP in solution with contrast-matched detergent. The first step of this process employed GNOM (35) to generate a pair-distance distribution function $P(r)$, which described the relative interatomic distances within the scattering particle. Scattering data over the range $0.0106 < Q < 0.585 \text{ \AA}^{-1}$ were used for the real space transformation and subsequent modeling, and provided a $P(r)$ curve with a single peak and D_{max} of 46 \AA . The R_g from the real space transformation was $16.7 \pm 0.2 \text{ \AA}$ with an I_0 of $0.610 \pm 0.001 \text{ cm}^{-1}$. The GNOM output was used for *ab initio* molecular shape generation with DAMMIF and DAMMIN (36,37). The $P(r)$ data were used as an input for fast DAMMIF modeling to create 17 initial dummy atom models (DAMs). These initial DAMs were aligned and averaged using DAMAVER (38), and one outlier from the 17 was discarded based on normalized spatial discrepancy (NSD) values, as its NSD value exceeded two standard deviations from the cluster mean (cluster NSD: 0.708 ± 0.018 ; outlier NSD: 0.749). After averaging in DAMAVER, the “damstart” (fixed-core) model was used for refinement with DAMMIN, yielding a single refined SANS envelope. Superimpositions of the SANS envelope with crystal structures were performed using SUPCOMB (39), which minimizes NSD to find the best alignment of the two models.

RESULTS

SANS analysis of *d*-MmIAP

SAXS measurements showed, as expected, strong scattering signal from DDM micelles that was similar with and without MmIAP, and initial attempts of SANS experiments using nondeuterated MmIAP, DDM, and D₂O/H₂O were un-

successful in isolating a signal for MmIAP unperturbed by scattering contributions from the surfactant (Fig. S2). Therefore, *d*-MmIAP was expressed and purified (Fig. S1) immediately before data collection, using established methods yielding active enzyme (14). Based on other studies (40), the average deuteration level under growth conditions is 70–75%. Scattering from the *d*-MmIAP protein-detergent complex produced a stronger signal overall as a result of the increased protein contrast relative to the solvent, but contributions from the detergent were still present in the net scattering profile. These results are observed in a comparison of the MmIAP-DDM complex versus *d*-MmIAP-DDM in the same DDM contrast-matched conditions (Fig. 1).

To achieve true extinction of any scattering contribution from DDM, a more refined approach was required. The individual contrast match points (CMPs) of hydrophobic DDM alkyl tails and hydrophilic maltoside headgroups are 2 and 48.5% D₂O, respectively, which are very far from the overall CMP of 22% D₂O. This, together with the similar size of both moieties and their distinctive location in a micelle core and shell produces significant residual scattering, even at 22% D₂O (Fig. 1). This problem can be resolved by raising the CMP of the DDM micelle core to 48.5% D₂O to match the shell by precisely blending 44% (w/v) tail-deuterated DDM (d25-DDM) with regular DDM (41). Under these complete matching conditions, scattering features from DDM micelles were rendered negligible (Fig. 1), which is readily apparent by the absence of a secondary maximum in the SANS profile.

The combination of deuterated protein and completely contrast-matched mixed micelles yielded an interpretable SANS profile for the enzyme without interference from buffer and detergent components (Figs. 1 and 2 A). Guinier analysis was performed on the low- Q scattering data defined by an upper limit of $Q \times R_g < 1.3$, and provided estimates of I_0 and R_g (Fig. 2 B). The measured R_g ($16.1 \pm 0.5 \text{ \AA}$), and a

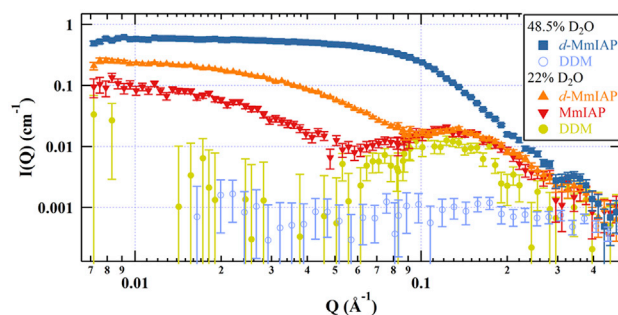


FIGURE 1 SANS contrast match point measurements for DDM micelles (yellow, ●), MmIAP with DDM (red, ▼), *d*-MmIAP with DDM (orange, ▲) in 22% D₂O, and mixed micelles (blue, ○) or *d*-MmIAP with DDM/d25-DDM mixed micelles (blue, ■) in 48.5% D₂O. Data for contrast-matched DDM micelles in 48.5% D₂O was reproduced from (41). To see this figure in color, go online.

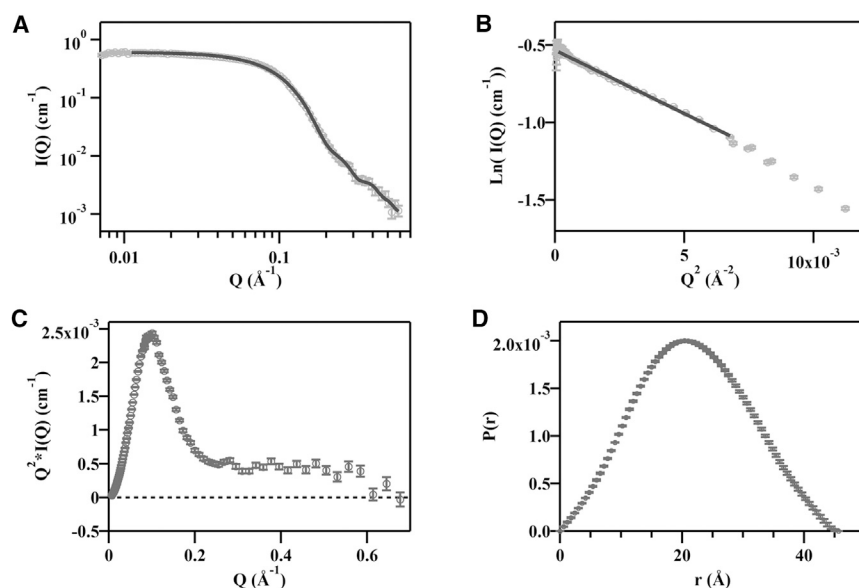


FIGURE 2 SANS data obtained for *d*-MmIAP with contrast-matched DDM/d25-DDM mixed micelles (48.5% D₂O). (A) A plot of the scattered intensity versus Q , a function of the scattering angle, with GNOM fit shown in solid line. (B) A Guinier plot of the low angle scattering data with a linear fit in the Guinier region shown as a solid line. (C) A Kratky plot of the same scattering data demonstrating the compact, folded shape of the particle. (D) A pair-distance distribution function $P(r)$ obtained from GNOM representing the distribution of real space distances between scattering centers within the particle.

Kratky plot illustrating the folded nature of the scattering object (Fig. 2 C), suggests that MmIAP is most likely monomeric with a compact, globular shape in detergent solution (42). The forward scattering intensity determined from the Guinier fit was $0.60 \pm 0.01 \text{ cm}^{-1}$. An indirect Fourier transform of the scattering data provided a plot describing the pair-distance distribution $P(r)$ of intramolecular distances within the particle, constrained by a maximum particle dimension of 46 \AA (Fig. 2 D). Molecular weight was estimated from the DAMMIN model and by the method described by Rambo and Tainer (43) (see Supporting Material for details). A summary of the physical parameters extracted from the SANS data in comparison with similar values obtained from the final SANS envelope and the PDB model (4HYC, chain A) is presented in Table 1. The combination of these results from SANS suggest a monomeric MmIAP size and shape without the formation of higher order oligomers in micellar solution.

Comparison with crystal structure and *ab initio* modeling

SANS profiles were calculated from available structures for pertinent enzymes (chain A from MmIAP PDB: 4HYC, 4HYD, 4HYG, and 4Y6K, and chain B, presenilin from γ -secretase PDB: 5A63, 5FN2, 5FN3, 5FN4, and 5FN5). The four MmIAP crystal structures are ~ 3.3 – 3.9 \AA resolution, represent three different space groups, different bound states (apo and inhibited), and are similar to each other with

root-mean square deviation (RMSD) of ~ 0.5 – 0.8 \AA . The five presenilin structures solved by cryo-electron microscopy are 4.0 – 4.3 \AA resolution, and represent four apo states, as well as one that is bound to an inhibitor. Presenilin shares just 15% identity with MmIAP yet pairwise RMSDs for the two different structures are ~ 2.5 – 3 \AA . CRYSON fits to the experimental data from representative members of each PDB group are shown in Fig. 3 A. The simulated scattering profiles for structural monomers are in relative agreement with the measured scattering profile of *d*-MmIAP in contrast-matched, mixed d25-DDM/DDM micelles (Fig. 3). Each structure appears somewhat larger than that measured in solution, denoted by the decrease in scattered intensity from the plateau at lower values of Q for the simulated SANS data compared with the measured data, but are much closer to the data than a hypothetical *d*-MmIAP dimer and tetramer (Fig. 3 A). The average R_g from the structure (19.4 \AA , Table 1) is also $\sim 3.4 \text{ \AA}$ larger than the R_g determined from a Guinier fit to the SANS data ($16.1 \pm 0.5 \text{ \AA}$).

Ab initio modeling from *d*-MmIAP SANS data with contrast-matched detergent recapitulates the overall agreement with the available structures. A representative scattering profile from the remaining DAMMIF models demonstrates strong agreement with the experimental data (Fig. 3 A) and the SANS profile of the DAMMIN-refined envelope was indistinguishable from this representative trace. The SANS envelope shown here has a protrusion that is consistent with the predicted position of the long helix 6, which contains the C-terminal YD motif, and a well leading

TABLE 1 Summary of Physical Parameters from the SANS Data, Reconstructed DAM, and the Related PDB: 4HYC:A

	Radius of Gyration (\AA)				D_{max} (\AA)			Volume (\AA^3)		
	GNOM	DAM	PDB		GNOM	DAM	PDB	SANS	DAM	PDB
Guinier	16.1 ± 0.5	16.7 ± 0.2	16.7	19.4	46.0	47.7	72.9	21,030	20,590	31,258

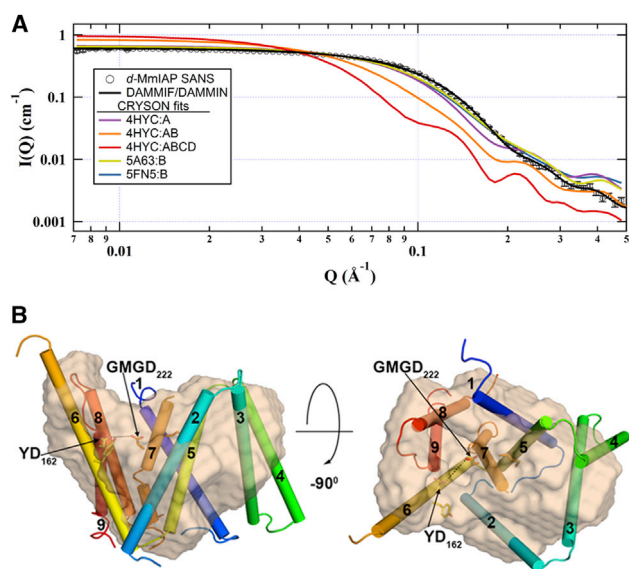


FIGURE 3 CRYSON results and comparison with SANS data. (A) Simulated SANS profiles from CRYSON for representative PDB entries related to IAPs. Scattering from a possible MmIAP dimer and tetramer were simulated using chains A and B from 4HYC, or chains A–D from 4HYC, respectively, demonstrating that higher ordered oligomers are not consistent with the observed scattering. (B) The *ab initio* model was overlaid with chain A from 4HYC to provide a three-dimensional structural comparison. TM helices numbered from 1 (N-terminus (blue)) to 9 (C-terminus (red)), and catalytic motif YD. GMGD is represented as sticks. To see this figure in color, go online.

to the general vicinity of the catalytic aspartates (Fig. 3 B). However, we note that not all 16 DAMs show exactly these features in the same location; thus, the fit shown here agrees with the SANS data, but this envelope is not the only possible model at this level of detail. The poorest fit is for helix 4, half of which appears to protrude beyond the SANS envelope in accordance with the larger R_g and D_{max} values (Table 1) and calculated scattering intensity at low- Q values.

DISCUSSION

Despite the increasing number of available membrane protein structures in the protein data bank determined by x-ray crystallography, NMR spectroscopy, and cryo-electron microscopy, the percentage remains very low compared with the total membrane-bound proteome, and determining the oligomerization state of such proteins in solution remains a major challenge (44–46). Here we used SANS to determine the molecular envelope and oligomerization state of an IAP in solution. Our strategy had three major components, 1) deuterating MmIAP during cell growth to increase the SANS signal from the enzyme, 2) utilizing 44% d25-DDM to match the CMP of the hydrophobic tail core with that of the headgroup of the DDM micelle, and 3) contrast matching the overall DDM micelle with 48.5% D₂O to leave only scattering from *d*-MmIAP.

The process of contrast matching to detect only the signal from the membrane protein is inherently challenging (47); micelle-micelle interaction or protein-protein interactions can corrupt low- Q data, and the residual signal from incompletely matched lipid head and tail components limit data interpretation to gross structural changes under defined experimental conditions. Typically, SANS studies of membrane proteins employ the average CMP for the solubilizing agent. For example, Bu et al. (48) overall contrast-matched the small unilamellar vesicles to detect a change in the oligomeric state of SecA upon nucleotide binding, and Zimmer et al. (49) used the average contrast match for DDM of 22% D₂O to detect differences between truncated and full-length potassium channel KcsA solubilized in DDM under different pH conditions. With our improved understanding of the detergent contributions to neutron scattering (41), reinspection of numerous SANS studies that utilize a similar strategy (49–54) suggests that the scattering profile exhibits contributions due to incompletely matched surfactant or lipid components. Thus, our recent efforts have been aimed at improving the contrast matching protocol by matching the hydrophobic tail of the detergent to its headgroup before contrast matching the overall micelle with D₂O. One prior study used an analogous strategy with sodium dodecyl sulfate (55), but to our knowledge, our study is the first such application to study a membrane enzyme solubilized in DDM, a milder detergent with a larger headgroup (45). The theoretical basis for the approach with DDM was recently reported (41), and resulted in a strong interpretable signal free of contribution from the detergent.

The *d*-MmIAP *ab initio* model in solution is consistent with an approximately spherical monomeric protein, not a dimer or higher ordered species suggested in earlier biochemical experiments for SPP and other human IAP family members. Interestingly, the experimentally determined R_g (16.1 ± 0.5 Å) from SANS is somewhat smaller than the calculated R_g (19.4 Å) from a monomer chain of crystalline MmIAP, indicating a more compact structure is present in solution. This finding agrees with the observation that crystallized MmIAP was trapped in an inactive conformation, with the two catalytic aspartates too far apart for catalysis. Detergent identity and concentration are well known to affect crystallization properties (56,57). In the case of the MmIAP crystal structure, perhaps the limited proteolytic digestion of the enzyme or mutations introduced to enhance crystallizability (24), led to a less compact bundle of transmembrane helices. Alternatively, the dynamic detergent micelles present during crystallization might affect the lattice (58–60), as would be expected for an α -helical membrane protein with predominantly membrane-immersed helices (61). Our sample for SANS was prepared using the same methods as for our enzymatic study where it is active for nearly a week after purification (14), suggesting our SANS envelope reflects that of an active

enzyme in detergent solution, but whether the protein remains a monomer in the presence of substrate is an open question for further study.

CONCLUSIONS

SANS analysis of *d*-MmIAP measured with fully contrast-matched detergent yields a molecular envelope consistent with a monomeric enzyme in solution. Comparison of the R_g value from SANS and previously reported crystal structure of an inactive IAP suggests the protein might form a more compact protein in solution, namely, tighter packing of the hydrophobic transmembrane helices. The finding that MmIAP is a monomer is consistent with the recent cryo-electron microscopy structure of presenilin in the context of γ -secretase, but differs from other experiments conducted with indirect biophysical or biochemical methods. The SANS approach and CMP strategy, used to study *d*-MmIAP in solution, should be applicable to study IAP structures in complex with substrates, other IP family proteins, and other well-behaved, detergent-solubilized membrane proteins.

SUPPORTING MATERIAL

Supporting Materials and Methods and three figures are available at [http://www.biophysj.org/biophysj/supplemental/S0006-3495\(17\)35097-X](http://www.biophysj.org/biophysj/supplemental/S0006-3495(17)35097-X).

AUTHOR CONTRIBUTIONS

Conceptualization, Methodology, R.C.O., V.S.U., K.L.W., and R.L.L.; Investigation, S.-H.N., R.C.O., and K.L.W.; Writing – Original Draft, S.-H.N., R.C.O., V.S.U., and R.L.L.; Writing – Review and Editing, S.-H.N., R.C.O., K.L.W., V.S.U., and R.L.L.; Funding Acquisition and Supervision, R.L.L., and V.S.U.

ACKNOWLEDGMENTS

This work was supported by a grant to R.L.L. from the National Science Foundation (NSF) (0845445). S.-H.N. acknowledges a travel grant from the College of Sciences, Georgia Tech to collect data at Oak Ridge National Laboratory. Neutron scattering studies at the CG-3 Bio-SANS instrument at the High-Flux Isotope Reactor and work in the Bio-Deuteration Laboratory of Oak Ridge National Laboratory were sponsored by the Office of Biological and Environmental Research and by the Scientific User Facilities Division, Office of Basic Energy Sciences, US Department of Energy (DOE). This work benefited from the use of the SasView application, originally developed under NSF award DMR-0520547. SasView also contains code developed with funding from the EU Horizon 2020 programme under the SINE2020 project grant 654000. This manuscript has been coauthored by UT-Battelle, LLC, under contract DE-AC05-00OR22725 with the DOE.

The US government retains and the publisher, by accepting the article for publication, acknowledges that the US government retains a nonexclusive, paid-up, irrevocable, worldwide license to publish or reproduce the published form of this manuscript, or allow others to do so, for US government purposes. DOE will provide public access to these results of federally sponsored research in accordance with the DOE Public Access Plan (<http://energy.gov/downloads/doe-public-access-plan>).

SUPPORTING CITATIONS

Reference (62) appears in the Supporting Material.

REFERENCES

- Brown, M. S., J. Ye, ..., J. L. Goldstein. 2000. Regulated intramembrane proteolysis: a control mechanism conserved from bacteria to humans. *Cell*. 100:391–398.
- Verhelst, S. H. L. 2017. Intramembrane proteases as drug targets. *FEBS J*. 284:1489–1502.
- Urban, S., and M. Freeman. 2002. Intramembrane proteolysis controls diverse signalling pathways throughout evolution. *Curr. Opin. Genet. Dev.* 12:512–518.
- Manolaridis, I., K. Kulkarni, ..., D. Barford. 2013. Mechanism of farnesylated CAAX protein processing by the intramembrane protease Rce1. *Nature*. 504:301–305.
- Erez, E., D. Fass, and E. Bibi. 2009. How intramembrane proteases bury hydrolytic reactions in the membrane. *Nature*. 459:371–378.
- Weihofen, A., K. Binns, ..., B. Martoglio. 2002. Identification of signal peptide peptidase, a presenilin-type aspartic protease. *Science*. 296:2215–2218.
- Lemberg, M. K., F. A. Bland, ..., B. Martoglio. 2001. Intramembrane proteolysis of signal peptides: an essential step in the generation of HLA-E epitopes. *J. Immunol.* 167:6441–6446.
- Fluhrer, R., G. Grammer, ..., C. Haass. 2006. A gamma-secretase-like intramembrane cleavage of TNFalpha by the GxGD aspartyl protease SPPL2b. *Nat. Cell Biol.* 8:894–896.
- McLauchlan, J., M. K. Lemberg, ..., B. Martoglio. 2002. Intramembrane proteolysis promotes trafficking of hepatitis C virus core protein to lipid droplets. *EMBO J*. 21:3980–3988.
- Weihofen, A., M. K. Lemberg, ..., B. Martoglio. 2003. Targeting presenilin-type aspartic protease signal peptide peptidase with gamma-secretase inhibitors. *J. Biol. Chem.* 278:16528–16533.
- Sato, T., A. C. Nyborg, ..., M. S. Wolfe. 2006. Signal peptide peptidase: biochemical properties and modulation by nonsteroidal anti-inflammatory drugs. *Biochemistry*. 45:8649–8656.
- Torres-Arancivia, C., C. M. Ross, ..., I. Ubarretxena-Belandia. 2010. Identification of an archaeal presenilin-like intramembrane protease. *PLoS One*. 5:e13072.
- Dang, S., S. Wu, ..., Y. Shi. 2015. Cleavage of amyloid precursor protein by an archaeal presenilin homologue PSH. *Proc. Natl. Acad. Sci. USA*. 112:3344–3349.
- Naing, S. H., K. M. Vukoti, ..., R. L. Lieberman. 2015. Catalytic properties of intramembrane aspartyl protease substrate hydrolysis evaluated using a FRET peptide cleavage assay. *ACS Chem. Biol.* 10:2166–2174.
- Gimpl, K., J. Klement, and S. Keller. 2016. Characterising protein/detergent complexes by triple-detection size-exclusion chromatography. *Biol. Proced. Online*. 18:4.
- Pérez, J., and A. Koutsioubas. 2015. Memprot: a program to model the detergent corona around a membrane protein based on SEC-SAXS data. *Acta Crystallogr. D Biol. Crystallogr.* 71:86–93.
- Bai, X. C., C. Yan, ..., Y. Shi. 2015. An atomic structure of human γ -secretase. *Nature*. 525:212–217.
- Miyashita, H., Y. Maruyama, ..., T. Iwatsubo. 2011. Three-dimensional structure of the signal peptide peptidase. *J. Biol. Chem.* 286:26188–26197.
- Cervantes, S., C. A. Saura, ..., G. Marfany. 2004. Functional implications of the presenilin dimerization: reconstitution of gamma-secretase activity by assembly of a catalytic site at the dimer interface of two catalytically inactive presenilins. *J. Biol. Chem.* 279:36519–36529.
- Herl, L., A. Lleo, ..., O. Berezovska. 2006. Detection of presenilin-1 homodimer formation in intact cells using fluorescent lifetime imaging microscopy. *Biochem. Biophys. Res. Commun.* 340:668–674.

21. Nyborg, A. C., L. Herl, ..., T. E. Golde. 2006. Signal peptide peptidase (SPP) dimer formation as assessed by fluorescence lifetime imaging microscopy (FLIM) in intact cells. *Mol. Neurodegener.* 1:16.
22. Nyborg, A. C., A. Y. Kornilova, ..., T. E. Golde. 2004. Signal peptide peptidase forms a homodimer that is labeled by an active site-directed gamma-secretase inhibitor. *J. Biol. Chem.* 279:15153–15160.
23. Schroeter, E. H., M. X. Ilagan, ..., R. Kopan. 2003. A presenilin dimer at the core of the gamma-secretase enzyme: insights from parallel analysis of Notch 1 and APP proteolysis. *Proc. Natl. Acad. Sci. USA.* 100:13075–13080.
24. Li, X., S. Dang, ..., Y. Shi. 2013. Structure of a presenilin family intramembrane aspartate protease. *Nature.* 493:56–61.
25. Breyton, C., F. Gabel, ..., C. Ebel. 2013. Small angle neutron scattering for the study of solubilised membrane proteins. *Eur Phys J E Soft Matter.* 36:71.
26. Trehwella, J. 2006. Neutrons reveal how nature uses structural themes and variation in biological regulation. *Physica B.* 385–386:825–830.
27. Lynn, G. W., W. Heller, ..., D. A. A. Myles. 2006. Bio-SANS - A dedicated facility for neutron structural biology at oak ridge national laboratory. *Physica B.* 385–386:880–882.
28. Heller, W. T., V. S. Urban, ..., D. A. Myles. 2014. The Bio-SANS instrument at the high flux isotope reactor of oak ridge national laboratory. *J. Appl. Cryst.* 47:1238–1246.
29. He, L. L., C. Do, ..., G. S. Smith. 2015. Corrections for the geometric distortion of the tube detectors on SANS instruments at ORNL. *Nucl. Instrum. Methods Phys. Res. Sect. A Accel. Spectrom. Detect. Assoc. Equip.* 775:63–70.
30. Arnold, O., J. C. Bilheux, ..., J. Zikovsky. 2014. Mantid-Data analysis and visualization package for neutron scattering and mu SR experiments. *Nucl. Instrum. Methods Phys. Res. Sect. A Accel. Spectrom. Detect. Assoc. Equip.* 764:156–166.
31. Petoukhov, M. V., D. Franke, ..., D. I. Svergun. 2012. New developments in the ATSAS program package for small-angle scattering data analysis. *J. Appl. Cryst.* 45:342–350.
32. Konarev, P. V., V. V. Volkov, ..., D. I. Svergun. 2003. PRIMUS: a Windows PC-based system for small-angle scattering data analysis. *J. Appl. Cryst.* 36:1277–1282.
33. Doucet, M., J. H. Cho, ..., A. Washinton. 2017. SasView version 4.1. <http://www.sasview.org/>.
34. Svergun, D. I., S. Richard, ..., G. Zaccai. 1998. Protein hydration in solution: experimental observation by x-ray and neutron scattering. *Proc. Natl. Acad. Sci. USA.* 95:2267–2272.
35. Svergun, D. 1992. Determination of the regularization parameter in indirect-transform methods using perceptual criteria. *J. Appl. Cryst.* 25:495–503.
36. Svergun, D. I. 1999. Restoring low resolution structure of biological macromolecules from solution scattering using simulated annealing. *Biophys. J.* 76:2879–2886.
37. Franke, D., and D. I. Svergun. 2009. DAMMIF, a program for rapid ab-initio shape determination in small-angle scattering. *J. Appl. Cryst.* 42:342–346.
38. Volkov, V. V., and D. I. Svergun. 2003. Uniqueness of ab initio shape determination in small-angle scattering. *J. Appl. Cryst.* 36:860–864.
39. Kozin, M. B., and D. I. Svergun. 2001. Automated matching of high- and low-resolution structural models. *J. Appl. Cryst.* 34:33–41.
40. Leiting, B., F. Marsilio, and J. F. O'Connell. 1998. Predictable deuteration of recombinant proteins expressed in *Escherichia coli*. *Anal. Biochem.* 265:351–355.
41. Oliver, R. C., S. V. Pingali, and V. S. Urban. 2017. Designing mixed detergent micelles for uniform neutron contrast. *J. Phys. Chem. Lett.* 8:5041–5046.
42. Glatter, O., and O. Kratky. 1982. *Small Angle X-ray Scattering*. Academic Press, Cambridge, MA.
43. Rambo, R. P., and J. A. Tainer. 2013. Accurate assessment of mass, models and resolution by small-angle scattering. *Nature.* 496:477–481.
44. Parker, J. L., and S. Newstead. 2016. Membrane protein crystallisation: current trends and future perspectives. *Adv. Exp. Med. Biol.* 922:61–72.
45. Privé, G. G. 2007. Detergents for the stabilization and crystallization of membrane proteins. *Methods.* 41:388–397.
46. le Maire, M., P. Champeil, and J. V. Moller. 2000. Interaction of membrane proteins and lipids with solubilizing detergents. *Biochim. Biophys. Acta.* 1508:86–111.
47. Hunt, J. F., P. D. McCrea, ..., D. M. Engelman. 1997. Assessment of the aggregation state of integral membrane proteins in reconstituted phospholipid vesicles using small angle neutron scattering. *J. Mol. Biol.* 273:1004–1019.
48. Bu, Z., L. Wang, and D. A. Kendall. 2003. Nucleotide binding induces changes in the oligomeric state and conformation of Sec A in a lipid environment: a small-angle neutron-scattering study. *J. Mol. Biol.* 332:23–30.
49. Zimmer, J., D. A. Doyle, and J. G. Grossmann. 2006. Structural characterization and pH-induced conformational transition of full-length KcsA. *Biophys. J.* 90:1752–1766.
50. Cardoso, M. B., D. Smolensky, ..., H. O'Neill. 2009. Insight into the structure of light-harvesting complex II and its stabilization in detergent solution. *J. Phys. Chem. B.* 113:16377–16383.
51. Johs, A., M. Hammel, ..., R. Prassl. 2006. Modular structure of solubilized human apolipoprotein B-100. Low resolution model revealed by small angle neutron scattering. *J. Biol. Chem.* 281:19732–19739.
52. Kumar-Singh, S., J. Theuns, ..., C. Van Broeckhoven. 2006. Mean age-of-onset of familial alzheimer disease caused by presenilin mutations correlates with both increased Abeta42 and decreased Abeta40. *Hum. Mutat.* 27:686–695.
53. Nogales, A., C. García, ..., J. González-Rodríguez. 2010. Three-dimensional model of human platelet integrin alphaIIb beta3 in solution obtained by small angle neutron scattering. *J. Biol. Chem.* 285:1023–1031.
54. Tang, K. H., V. S. Urban, ..., R. E. Blankenship. 2010. SANS investigation of the photosynthetic machinery of *Chloroflexus aurantiacus*. *Biophys. J.* 99:2398–2407.
55. Clifton, L. A., C. L. Johnson, ..., J. H. Lakey. 2012. Low resolution structure and dynamics of a colicin-receptor complex determined by neutron scattering. *J. Biol. Chem.* 287:337–346.
56. Anandan, A., and A. Vrielink. 2016. Detergents in membrane protein purification and crystallisation. *Adv. Exp. Med. Biol.* 922:13–28.
57. Seddon, A. M., P. Curnow, and P. J. Booth. 2004. Membrane proteins, lipids and detergents: not just a soap opera. *Biochim. Biophys. Acta.* 1666:105–117.
58. Grishammer, R. 2017. New approaches towards the understanding of integral membrane proteins: a structural perspective on G protein-coupled receptors. *Protein Sci.* 26:1493–1504.
59. Moraes, I., G. Evans, ..., P. D. S. Stewart. 2014. Membrane protein structure determination - the next generation. *Biochim. Biophys. Acta.* 1838 (1 Pt A):78–87.
60. Wiener, M. C. 2004. A pedestrian guide to membrane protein crystallization. *Methods.* 34:364–372.
61. Schulz, G. E. 2011. A new classification of membrane protein crystals. *J. Mol. Biol.* 407:640–646.
62. Zaccai, N. R., I. N. Serdyuk, and J. Zaccai. 2017. *Methods in Molecular Biophysics*. Cambridge University Press, Cambridge, UK.